Virtual Ventricular Wall: Effects of Pathophysiology and Pharmacology on Transmural Propagation

Oleg V. Aslanidi[1], Jennifer L. Lambert[2], Neil T. Srinivasan[2] and Arun V. Holden[1]

[1] School of Biomedical Sciences, University of Leeds, LS2 9JT, UK
[2] School of Medicine, University of Leeds, LS2 9JT, UK
oleg@cbiol.leeds.ac.uk
http://cbiol.leeds.ac.uk

Abstract. Effects of pathophysiological conditions and pharmacological intervention on transmural propagation are computed for the virtual ventricular wall. ST depression during sub-endocardial ischaemia and unidirectional functional block in the vulnerable window during Class III drug action are explained by changes induced in the transmural dispersion of action potential duration.

1 Introduction

Electrophysiological recordings from cells and tissue isolated from endocardial, mid-myocardial (M-cell) and epicardial regions of the ventricular wall show marked transmural differences. These include differences in action potential (AP) shape and duration [1], as well as differential responses to changes in pacing cycle length, pharmacological intervention and pathophysiological conditions (e.g., ischaemia). The importance of dispersion of action potential duration (APD) for the initiation of arrhythmias is well recognized [2-4], and the respective transmural differences can be a potent arrhythmogenic source. Even if cell coupling reduces the transmural differences, they can be enhanced by pathophysiology, such as ischaemia [5], or by pharmacological blocking of repolarising K^+ currents (primarily I_{Kr} and I_{Ks}), which can increase the transmural APD dispersion and trigger re-entrant arrhythmias [6].

We use a computational model – virtual ventricular wall – to study electrophysiological changes of the transmural APD dispersion in response to pathophysiological conditions and pharmacological intervention – primarily, ST depression during sub-endocardial ischaemia and unidirectional propagation block in the vulnerable window (VW) during action of Class III drugs.

The link between the transmural heterogeneity of the ventricular tissue and clinically recorded electrocardiograms (ECGs) under normal and abnormal conditions has been explored recently: Antzelevitch et al. [7,8] related transmural APD differences to development of QT dispersion, and Gima and Rudy [9] explained how the APD dispersion accounts for ST elevation during global ischaemia [10]. We use a similar approach to dissect the electrophysiological mechanisms of ST depression during sub-endocardial ischaemia. Although depression of the ST-segment in ECGs is used clinically as an index of sub-endocardial ischaemia [11,12], the impact of the associated transmural electrophysiological changes is still not known.

A.F. Frangi et al. (Eds.): FIMH 2005, LNCS 3504, pp. 162 – 171, 2005.

Experiments suggest that ventricular tissues with large transmural differences in APD are more vulnerable to re-entry, and clinical studies show that pharmacological treatment that increases the APD dispersion can be proarrhythmic [6,13]. We compare electrophysiological properties of tissues treated with two different Class III drugs: amiodarone and d-sotalol. Proarrhythmic d-sotalol increases the transmural heterogeneity by preferentially increasing APD in M-cells [14,15], whereas amiodarone, the safest among Class III drugs, decreases the heterogeneity by increasing APD in endo- and epicardial cells [6]. However, electrophysiological mechanisms underlying the low arrhythmogenicity of amiodarone at the tissue level are poorly understood. We study the differential effects of the Class III drugs on transmural propagation, APD dispersion and vulnerable properties of the virtual ventricular wall.

2 Virtual Ventricular Wall

Virtual ventricular tissues are physiologically detailed reaction-diffusion models of ventricular tissues, that have proved to be an effective tool for simulating normal and abnormal ventricular propagation patterns, and for proposing hypotheses that can be tested experimentally [4,16-18]. In this paper we study transmural propagation in virtual ventricular wall consisting of three compact regions: endo-, M- and epicardial.

A one-dimensional (1D) model describing profiles of the membrane voltage, V (mV), through the virtual wall is based on the nonlinear cable equation [4, 16-18]:

$$\frac{\partial V}{\partial t} = \frac{\partial}{\partial x}\left(D \frac{\partial V}{\partial x} \right) - I_{\mathbf{ion}} . \qquad (1)$$

Here $0 \le x \le L$ is spatial coordinate through the virtual wall (mm), t is time (ms). L = 15 mm is the thickness of the virtual wall. D is the effective diffusion coefficient ($mm^2\ ms^{-1}$), that characterizes electrotonic spread of voltage, primarily through the intercellular resistive gap junctions. I_{ion} is the total membrane ionic current ($\mu A\ \mu F^{-1}$). The latter can be described in biophysical detail by the Luo-Rudy dynamic (LRd) ventricular cell model [19], which includes equations for time and voltage-dependent current flow through ion channels, pumps and exchangers in the cell membrane, as well as for Ca^{2+} dynamics within the cell.

Note that "1D virtual wall" refers to an idealization of the real 3D ventricular wall. Similar to the transmural wedge experiments [7, 8] and previous modelling studies [9], our simulations correspond to the situation during a normal heart-beat, where the Purkinje system ensures near-simultaneous excitation of the endocardium, resulting in a planar transmural wave-front parallel to the endocardial surface. 1D model is sufficient for simulating such a planar wave.

Transmural differences in the density of two repolarizing ionic currents, the slow-delayed rectifier potassium current I_{Ks} ($\mu A\ \mu F^{-1}$) and the transient outward potassium current I_{to} ($\mu A\ \mu F^{-1}$), through the virtual ventricular wall are introduced to represent three cell types: endo-, M- and epicardial [9]. Primarily, the density ratio I_{Ks}:I_{Kr} (here I_{Kr} is the rapid-delayed rectifier potassium current) is 11:1, 4:1 and 35:1, and maxi-

mum conductance of the I_{to} current is 0.0, 0.2125 and 0.25 mS μF^{-1} for endo-, M- and epicardial cells, respectively.

For geometric simplicity we assume that each cell type composes a uniform region occupying a third of the wall. As the exact proportion of endo-, M- and epicardial cells within the wall is not known, this assumption constitutes a first approximation of the transmural cellular structure. It also allows direct comparison of our simulations with the results on ST elevation in globally ischaemic ventricular wall [9]. The diffusion coefficient is set to a uniform value of 0.06 $mm^2\ ms^{-1}$ through the whole wall, except for a 5-fold decrease at the boundary between M- and epicardial regions [9], giving a solitary action potential transmural propagation velocity of 0.45 $m\ s^{-1}$ and a transmural propagation time of ~33 ms.

The equation (1) is solved numerically using the explicit Euler method with time step Δt = 0.005 ms and space step Δx = 0.1 mm. The endocardial end of the wall is stimulated 5 times by 0.5 ms, –100 $\mu A\ \mu F^{-1}$ current pulse stimuli at a basic cycle length (BCL) of 500 ms, leading to the transmural action potential propagation. Ectopic (S2) stimuli are applied at different time intervals following the last AP, resulting in either propagation failure, unidirectional functional propagation block or bidirectional propagation. Vulnerable window is defined as the range of S2 intervals leading to the unidirectional block (see in Fig. 1).

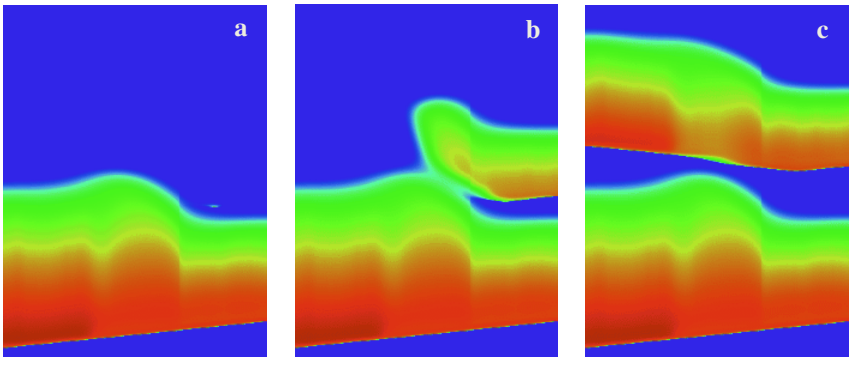

Fig. 1. Transmural AP propagation and VW definition in the virtual ventricular wall. The wall is stimulated from the endocardial end (at the left), leading to the AP propagation. Following S2 stimulation with different timing results in either (**a**) propagation failure for S2 = 160 ms, (**b**) unidirectional block for S2 = 180 ms or (**c**) bidirectional propagation for S2 = 200 ms. Space-time plots are shown, the membrane voltage is colour-coded using the standard rainbow palette. Each panel presents 400 ms of activity in 15 mm thick wall. In this illustration the S2 stimuli are applied to the epicardial region at x = 12 mm

Sub-endocardial ischaemia is an ischaemic region of spatial extent $l < L$ ($l = L$ corresponds to global ischaemia), in which the ATP concentration (mM), the extracellular potassium concentration $[K^+]_o$ (mM) and pH are changed [9,20]. In the normal conditions ATP = 10 mM, $[K^+]_o$ = 4.0 mM and pH = 7.5, in the ischaemic conditions ATP = 3 mM, $[K^+]_o$ = 10.0 mM and pH = 6.5. Transmural differences in

the density of ATP-sensitive potassium current $I_{K(ATP)}$ (μA μF^{-1}) are also accounted for by varying the half-saturation coefficient for this current, k_{ATP} (mM): k_{ATP} equals 0.0625, 0.125 and 0.25 mM in the endo-, M- and epicardial regions, respectively [9].

The effects of amiodarone and d-sotalol are incorporated as changes in the density of the rapid-delayed rectifier potassium current I_{Kr} (μA μF^{-1}) – the primary target for the Class III drug action – and the L-type depolarizing calcium current $I_{Ca,L}$ (μA μF^{-1}), which reproduces relative alterations of APD in the three cell types [6,14,15]. For the d-sotalol model I_{Kr} is depressed by 40% in endo-, by 100% in M-cell and by 65% in the epicardial region; for the amiodarone model I_{Kr} is uniformly depressed by 50% throughout the wall and $I_{Ca,L}$ is depressed by 40% in the M-cell region.

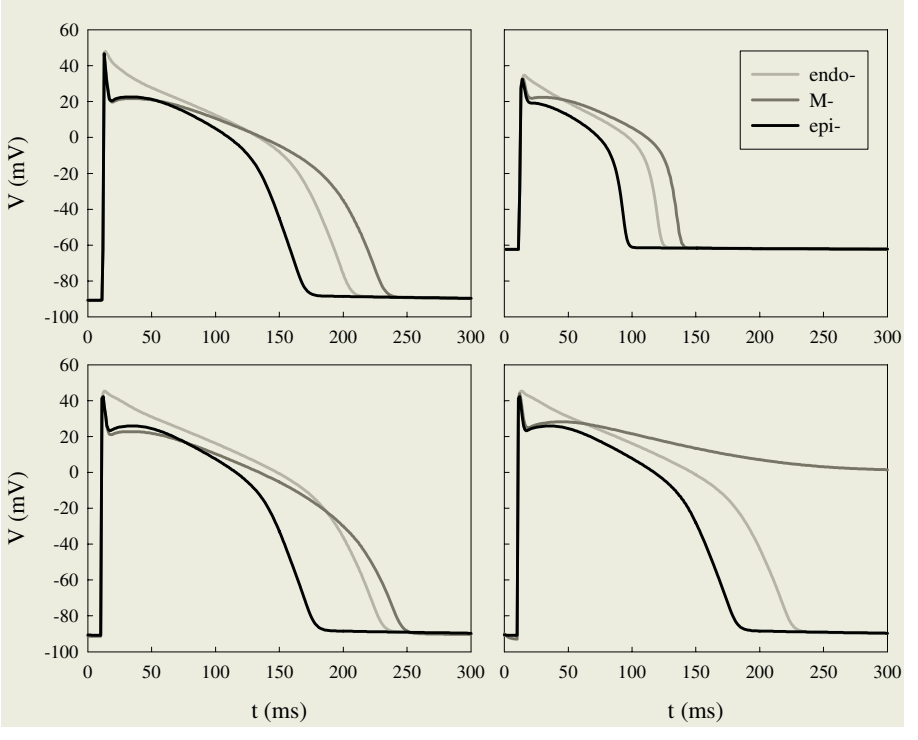

Fig. 2. Action potentials in endo-, M- and epicardial cells. APs for each of the three cell types are shown under the normal (top left) and ischaemic (top right) conditions, and under the effects of amiodarone (bottom left) and d-sotalol (bottom right)

Single-cell action potentials generated by endo-, M- and epicardial cells under various conditions studied in this paper are illustrated in Fig. 2.

The extracellular potential generated by the spatial membrane voltage distribution $V(x, t)$ within the 1D virtual ventricular wall is estimated using the expression [9]:

$$\Phi_e(x^*,t) = -K\int \frac{\partial V(x,t)}{\partial x}\cdot\frac{\partial}{\partial x}\left(\frac{1}{x^*-x}\right)dx\,. \tag{2}$$

Here K = 1.89 mm^2 is a positive constant, x^* = 20 mm is the distance from epicardial end of the tissue to an in line "electrode" site. The time profile of Φ_e constitutes an approximation for the ventricular component of the ECG – pseudo-ECG.

3 Results

3.1 Pathophysiology

Our simulations have separated the spatial and cellular mechanisms of ST depression caused by transmural AP propagation through a heterogeneous virtual ventricular wall during sub-endocardial ischaemia. ST depression results from predominantly positive transmural spatial gradients in the membrane voltage, $\partial V/\partial x$, and hence, in negative values of the integral Φ_e (2), during ventricular repolarization (Fig. 3). The gradients are produced by an abnormal transmural repolarization sequence caused by a decrease of APD in the ischaemic region. ST depression is facilitated by elevation of the pseudo-ECG baseline (see in Fig. 3), which results from a negative spatial gradient of the resting membrane potential between the normal and the ischaemic regions.

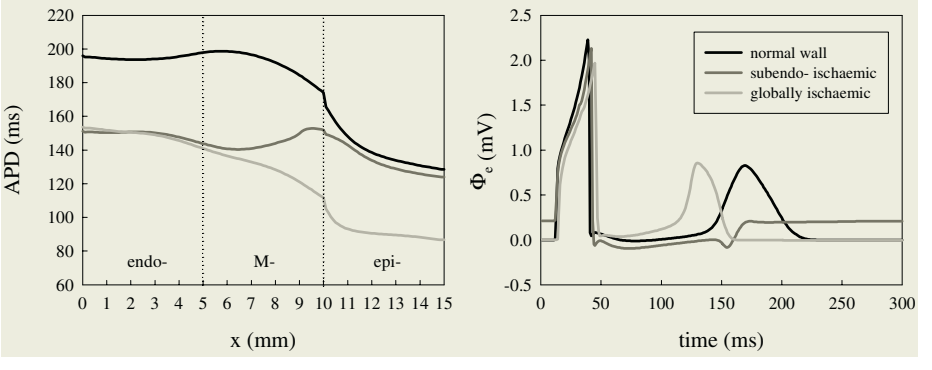

Fig. 3. Transmural distributions of APD in the normal, globally ischaemic and sub-endocardially ischaemic virtual ventricular walls (left), and respective pseudo-ECGs (right). Depth of the sub-endocardial ischaemia is l = 10 mm, such that the ischaemic region extends over the whole endocardial and M-cell regions, which results in decrease of APD

The cellular mechanisms of ST depression can be dissected by simulating separate components of the sub-endocardial ischaemia – acidosis, anoxia and hyperkalaemia. Our simulations show that sub-endocardial elevation of $[K^+]_o$ alone results in the transmural APD dispersion leading to ST-depression, whereas both sub-endocardially low pH and low ATP generate transmural APD distributions and ECG patterns re-

sembling those of the normal virtual wall (Fig. 4). We conclude that the primary cellular mechanism underlying ST depression is sub-endocardial hyperkalaemia – elevation of the extracellular potassium concentration $[K^+]_o$. Its effects on the electrophysiological properties of the ventricular wall are mediated through the K^+-sensitive membrane currents regulating the cellular AP shape and duration.

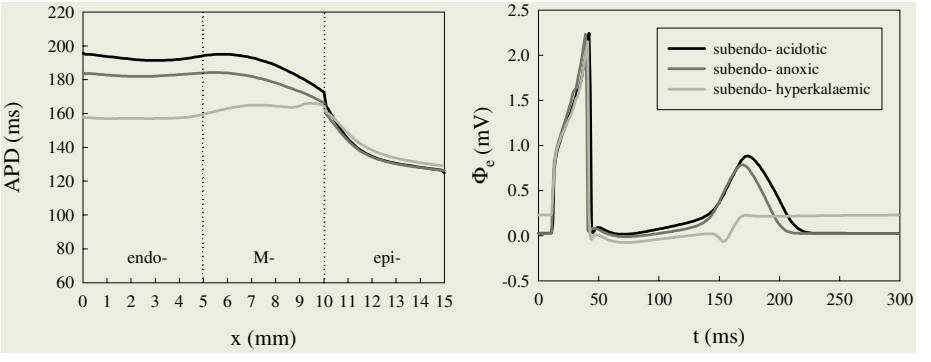

Fig. 4. Role of the ischaemic components – acidosis, anoxia and hyperkalaemia – in ST depression. Transmural distributions of APD (left) and pseudo-ECGs (right) are shown. l = 10 mm

3.2 Pharmacology

Fig. 1 illustrates AP propagation through the virtual ventricular wall and defines the vulnerable window. VWs computed for the walls treated with amiodarone and d-sotalol are shown in Fig. 5. The shape and extent of the VWs demonstrate clear correlation with the respective transmural APD dispersions within the wall. As d-sotalol increases the APD dispersion by predominant increase of APD in M-cells, the VW in

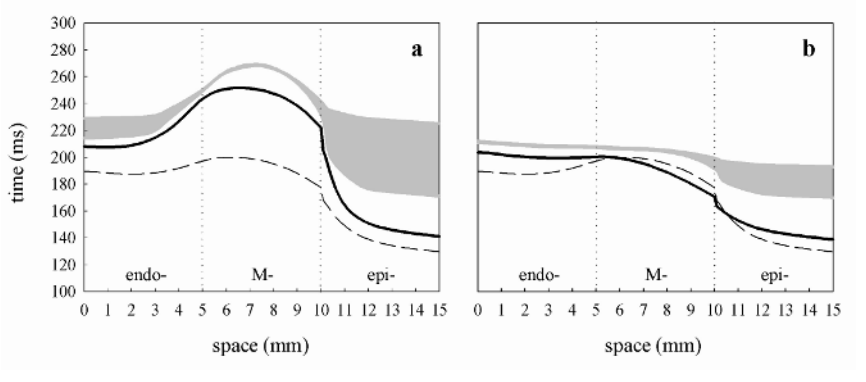

Fig. 5. Effects of (**a**) d-sotalol and (**b**) amiodarone on the virtual ventricular wall. Spatial distributions of APD through the normal wall (dashed line) and the wall treated by the drugs (solid lines) are shown along with the respective VWs (gray areas)

the endo- and epicardial regions, where unidirectional block persists until the M-cell region is fully repolarized, is wide. Amiodarone, however, decreases the dispersion by prolonging APD in endo- and epicardial cells and decreasing APD in M-cells, which results in a narrow VW similar to that of the normal tissue. Pacing the virtual wall at different BCL shows that the transmural APD dispersion is larger at low rates, especially with d-sotalol (Fig. 6).

We conclude that an electrophysiological explanation for the safety of amiodarone in comparison to other Class III drugs lies in relatively low transmural APD dispersion leading to narrow vulnerable window, and hence, low probability of unidirectional block (which can lead to initiation of re-entry in 2D and 3D) in the ventricular wall. Our simulations also show that APD change in M-cells is the major contributor to the transmural dispersion of repolarization, and hence, extent of the VW.

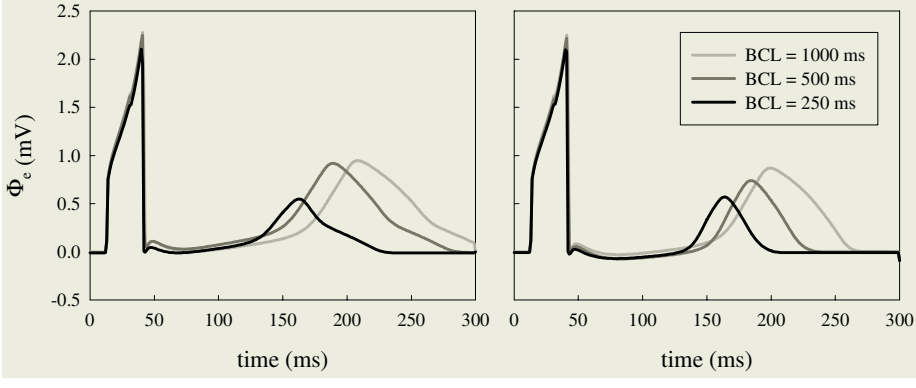

Fig. 6. Effects of BCL on the transmural APD dispersion. Pseudo-ECGs corresponding to the transmural AP propagation are computed for the virtual wall treated with d-sotalol (left) and amiodarone (right). T-wave prolongation is an index of increase in the APD dispersion [15]

4 Human Model

Although the LRd is the most experimentally validated of all cardiac cell models, it is adopted to description of AP properties in guinea-pig ventricular cells. However, clinical studies are performed on human patients, and hence, an adequate model of human cells, which accounts for the transmural variations, is required to compare computational results to these data. Such a model has been developed recently [21].

We use the equation (1) along with the description of the ionic current I_{ion} provided by the model [21] for endo-, M- and epicardial cells in order to simulate human virtual ventricular wall. The computational set-up is similar to that used in case of the LRd cellular models. As the human cell models have little difference in APD between the endo- and epicardial cells, the 1D virtual human wall does not generate a positive T-wave in the pseudo-ECG (2). Therefore, simulating ST-depression with this model is not feasible (as the ST-segment cannot be defined).

Results of simulating the effects of Class III drugs on the human virtual wall are illustrated in Fig. 7. The model reproduces the effects of d-sotalol and amiodarone on the APD dispersion, as seen in our LRd-based simulations, but the resultant VWs are very narrow (< 1 ms) throughout the virtual wall. We use dynamic restitution curves for single endo-, M- and epicardial cells to test rate-dependence of the APD dispersion. Fig. 8 shows that the transmural APD dispersion is large with d-sotalol and relatively small with amiodarone at all tested rates, which is in agreement with the experiments [15]. However, contrary to the experiments [15], the APD dispersion between the model endo-, M- and epicardial cells [21] does not substantially change with increasing BCL in the range from 1 to 10 seconds (see in Fig. 8).

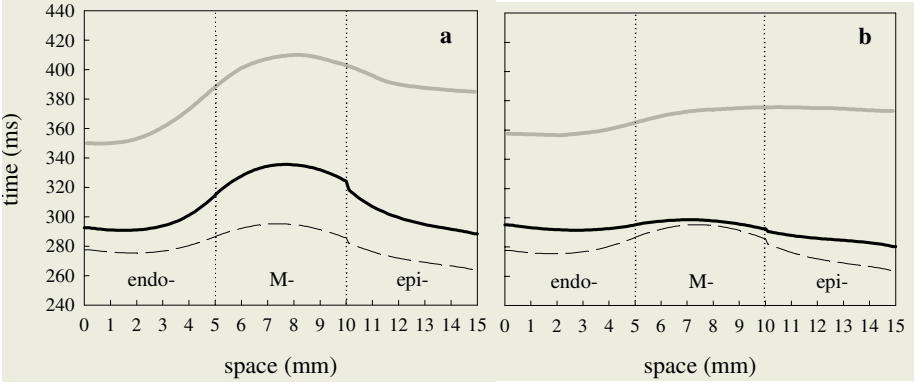

Fig. 7. Effects of (**a**) d-sotalol and (**b**) amiodarone on the human virtual ventricular wall. Spatial distributions of APD through the normal wall (dashed line) and the wall treated the drugs (solid lines) are shown along with the respective VWs (narrow gray areas)

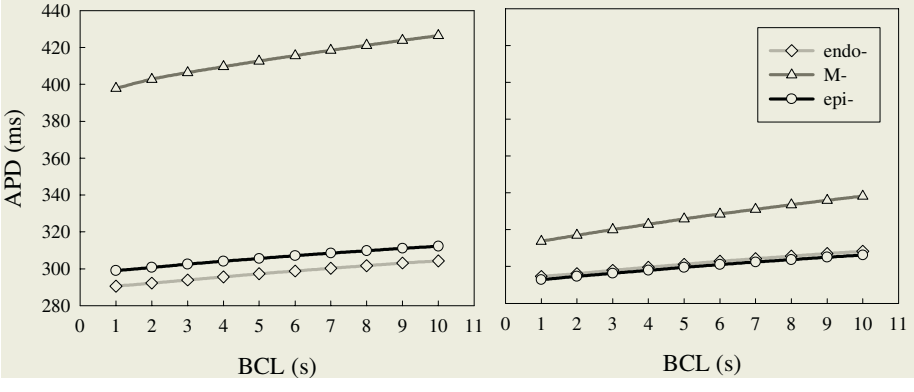

Fig. 8. Effects of BCL on APD in single human endo-, M- and epicardial cells treated with d-sotalol (left) and amiodarone (right). APD is measured after the cells are paced 5 times

5 Conclusion

We conclude that the effects of pathophysiology (sub-endocardial ischaemia) and pharmacology (Class III drugs) on the transmural propagation can be explained by changes in the transmural APD dispersion leading, primarily, to ST depression and increase of the vulnerable window in the virtual ventricular wall. ST depression results from relative changes of APD in endo-, M- and epicardial cells unequally effected by the ischaemia, and the increase/decrease of the tissue vulnerability in response to d-sotalol/amiodarone results from respective changes in the APD dispersion and probability of the unidirectional propagation block. Although our computational model has proved to be an effective tool for studying these effects, it cannot be used for simulating non-planar transmural or intramural waves, such as re-entrant vortexes [22,23]. Development of 2D and 3D models constitutes the next step of our research.

Acknowledgements

This research was funded by the MRC and EPSRC (UK).

References

1. Bryant, S.M., Wan, X., Shipsey, S.J. Hart, G. Regional differences in the delayed rectifier current (I_{Kr} and I_{Ks}) contribute to the differences in action potential duration in basal left ventricular myocytes in guinea-pig. Cardiovasc. Res. 40 (1998), 322-331.
2. Han, J., Moe, G.K. Nonuniform recovery of excitability in ventricular muscle. Circ. Res. 14 (1964), 44-60.
3. Burton, F.L., Cobbe, S.M. Dispersion of ventricular repolarization and refractory period. Cardiovasc. Res. 50 (2001), 10-23.
4. Clayton, R.H., Holden, A.V. Propagation of normal beats and re-entry in a computational model of ventricular cardiac tissue with regional differences in action potential shape and duration. Prog. Biophys. Mol. Biol. 85 (2004), 473-499.
5. Viswanathan, P.C., Rudy, Y. Cellular arrhythmogenic effects of congenital and acquired long-QT syndrome in the heterogeneous myocardium. Circulation 101 (2000), 1192-1198.
6. Akar, F.G., Yan, G.-X., Antzelevitch, C., Rosenbaum, D.S. Unique topographical distribution of M cells underlies re-entrant mechanism of Torsade de Pointes in the Long-QT syndrome. Circulation 105 (2002), 1247-1253.
7. Antzelevitch, C., Shimizu, W., Yan, G.X., Sicouri, S., Weissenburger, J., Nesterenko, V.V., Burashnikov, A., Di Diego, J., Saffitz, J., Thomas, G.P. The M cell: its contribution to the ECG and to normal and abnormal electrical function of the heart. J. Cardiovasc. Electrophysiol. 10 (1999), 1124-1152.
8. Antzelevitch, C., Yan, G.X., Shimizu, W. Transmural dispersion of repolarization and arrhyth-mogenicity: the Brugada syndrome versus the long QT syndrome. J. Electrocardiol. 32 (1999), 158-165.
9. Gima, K., Rudy Y. Ionic current basis of electrocardiographic waveforms – a model study. Circ. Res. 90 (2002), 889-896.
10. Kleber, A.G. ST-segment elevation in the electrocardiogram: a sign of myocardial ischaemia. Cardiovasc. Res. 45 (2000), 111-118.

11. Li, D., Li, C.Y., Yong, A.C., Kilpatrick, D. Source of electrocardiographic ST changes in subendocardial ischemia. Circ. Res. 82 (1998), 957-970.
12. Horacek, B.M., Wagner, G.S. Electrocardiographic ST-segment changes during acute myocardial ischemia. Card. Electrophysiol. Rev. 6 (2002), 196-203.
13. Huikuri, H.V., Castellanos, A., Myerburg, R.J. Sudden death due to cardiac arrhythmias. N. Engl. J. Med. 345 (2001), 1473-1482.
14. Sicouri, S., Moro, S., Litovsky, S., Elizari, M.V., Antzelevitch, C. Chronic amiodarone reduces transmural dispersion of repolarization in the canine heart. J. Cardiovasc. Electrophysiol 8 (1997), 1269-1279.
15. Drouin, E., Lande, G., Charpentier, F. Amiodarone reduces transmural heterogeneity of repolarization in the human heart. J. Am. Coll. Cardiol.32 (1998), 1063-1067.
16. Clayton, R.H., Holden, A.V. Computational framework for simulating the mechanisms and ECG of re-entrant ventricular fibrillation. Physiol. Meas. 23 (2002), 707-726.
17. Kohl, P., Noble, D., Winslow, R.L. Hunter, P.J. Computational modelling of biological systems: tools and visions. Philos. Trans. Roy. Soc. A 358 (2000), 579-610.
18. Aslanidi, O.V., Bailey, A., Biktashev, V.N., Clayton, R.H., Holden, A.V. Enhanced self-termination of re-entrant arrhythmias as a pharmacological strategy for antiarrhythmic action. Chaos 12 (2002), 843-851.
19. Luo, C.H., Rudy Y. A dynamic model of the cardiac ventricular action potential. I. Simula-tions of ionic currents and concentration changes. Circ. Res. 74 (1994), 1071-1096.
20. Shaw, R.M., Rudy, Y. Electrophysiologic effects of acute myocardial ischaemia: a theoreti-cal study of altered cell excitability and action potential duration. Cardiovasc. Res. 35 (1997), 256-272.
21. ten Tusscher, K.H., Noble, D., Noble, P.J., Panfilov, A.V. A model for human ventricular tissue. Am. J. Physiol. Heart Circ. Physiol. 286 (2004), H1573-1589.
22. Hyatt, C.J., Mironov, S.F., Wellner, M., Berenfeld, O., Popp, A.K., Weitz, D.A., Jalife, J., Pertsov, A.M. Synthesis of voltage-sensitive fluorescence signals from three-dimensional myocardial activation patterns. Biophys. J. 85 (2003), 2673-2683.
23. Clayton, R.H., Holden, A.V. Effect of regional differences in cardiac cellular electrophysiology on the stability of ventricular arrhythmias: a computational study. Phys. Med. Biol. 48 (2003), 95-111.